RECEIVED BY OSTI JAN 27 1986

CONF-8508153--3

LATTICE THERMAL EXPANSION EFFECTS IN PURE AND DOPED CORDIERITE BY TIME-OF-FLIGHT NEUTRON DIFFRACTION*

P. K. Predecki and J. Haas
University of Denver
Denver, CO 80208

and

J. Faber, Jr. and R. L. Hitterman
Materials Science and Technology Division
Argonne National Laboratory
Argonne, IL 60439

CONF-8508153--3

DE86 005547

FINAL

October 1985

The submitted manuscript has been authored by a contractor of the U. S. Government under contract No. W-31-109-ENG-38. Accordingly, the U. S. Government retains a nonexclusive, royalty-free license to publish or reproduce the published form of this contribution, or allow others to do so, for U. S. Government purposes.

DISCLAIMER

This report was prepared as an account of work sponsored by an agency of the United States Government. Neither the United States Government nor any agency thereof, nor any of their employees, makes any warranty, express or implied, or assumes any legal liability or responsibility for the accuracy, completeness, or usefulness of any information, apparatus, product, or process disclosed, or represents that its use would not infringe privately owned rights. Reference herein to any specific commercial product, process, or service by trade name, trademark, manufacturer, or otherwise does not necessarily constitute or imply its endorsement, recommendation, or favoring by the United States Government or any agency thereof. The views and opinions of authors expressed herein do not necessarily state or reflect those of the United States Government or any agency thereof.

MASTER

Submitted to the 34th Annual Denver X-ray Conference, August 5-9, 1985, Snowmass, CO; to be published in Advances in X-ray Analysis, Vol. 29.

*Work supported by Division of Basic Energy Sciences, U.S. Department of Energy, Washington, D.C., on Grant #DE-FG02-84ER45053 and under Contract W-31-109-Eng-38.

DISTRIBUTION OF THIS DOCUMENT IS UNLIMITED

LATTICE THERMAL EXPANSION EFFECTS IN PURE AND DOPED CORDIERITE BY TIME-OF-FLIGHT NEUTRON DIFFRACTION*

P. K. Predecki and J. Haas
University of Denver
Denver, CO 80208

and

J. Faber, Jr. and R. L. Hitterman
Materials Science and Technology Division
Argonne National Laboratory
Argonne, IL 60439

FINAL

October 1985

The submitted manuscript has been authored by a contractor of the U. S. Government under contract No. W-31-109-ENG-38. Accordingly, the U. S. Government retains a nonexclusive, royalty-free license to publish or reproduce the published form of this contribution, or allow others to do so, for U. S. Government purposes.

Submitted to the 34th Annual Denver X-ray Conference, August 5-9, 1985, Snowmass, CO; to be published in Advances in X-ray Analysis, Vol. 29.

*Work supported by Division of Basic Energy Sciences, U.S. Department of Energy, Washington, D.C., on Grant #DE-FG02-84ER45053 and under Contract W-31-109-Eng-38.

LATTICE THERMAL EXPANSION EFFECTS IN PURE AND DOPED CORDIERITE BY TIME-OF-FLIGHT NEUTRON DIFFRACTION*

P. K. Predecki and J. Haas
University of Denver, Denver, CO 80208
and
J. Faber, Jr. and R. L. Hitterman
Argonne National Laboratory, Argonne, IL 60439

ABSTRACT

The thermal expansion behavior of pure, Ge-doped and Li-doped hexagonal cordierites with respective compositions: $2MgO\ 2Al_2O_3\ 5SiO_2$, $2MgO\ 2Al_2O_3\ 4SiO_2\ GeO_2$, and $2MgO\ (2+x)Al_2O_3\ (5-2x)SiO_2\ xLi_2O$ with x = .174, was investigated using time-of-flight neutron powder diffraction at temperatures from 22 to 750°C in vacuum. The data were refined in space group P6/mcc using the Rietveld method. The lattice thermal expansion curves of all 3 samples were quite similar. The negative c axis expansion is associated with (1) displacement of the T_2 cations generally toward the c axis channels and (2) changes in the distortion of the coupled T_1/M tetrahedra/octahedra in the structure. Both contributions were present in all 3 samples but the first was more dominant in the Ge doped sample. The nature and origin of the distortions in T_1 and M are discussed.

INTRODUCTION

Cordierite is a magnesium-aluminum-silicate with the formula $2MgO\ 2Al_2O_3\ 5SiO_2$. It exists in two stable structural forms: (1) the high temperature hexagonal form with space group P6/mcc[2] isostructural with beryl, stable from 1450-1460°C (the melting point),[1] also known as indialite and (2) the slightly distorted and ordered orthorhombic form with space group Cccm,[3],[4] stable below 1450°C. The hexagonal form can also be formed at lower temperatures by devitrifying a glass of cordierite composition at temperatures near 1000°C.[5] The transformation of this hexagonal form to the orthorhombic follows a TTT type of behavior and is very slow below 1100°C: after 200 hrs at 1100°C the structure is still hexagonal.[6] On devitrifying the glass at 980°C the first phase to form is a metastable stuffed β-quartz structure of cordierite composition[5] also referred to as μ-cordierite.[7] After about 2 hrs at 980°C this transforms to the hexagonal form which is then stable for an indefinitely long period of time.[5]

In this study, only the low temperature hexagonal form was investigated. The objective was to gain an understanding of the negative c axis

*Work supported by Division of Basic Energy Sciences, DOE, Washington, D.C. on grant # DE-FG02-84ER45053.

expansion exhibited by this structure and the effect of cation dopants on the expansion mechanism.

EXPERIMENTAL

Samples were prepared from the component high purity oxide powders (mostly > 99.999%) correcting for moisture present in these powders. Compositions were, pure: $2MgO\ 2Al_2O_3\ 5SiO_2$, Li-doped: $2MgO\ (2+x)Al_2O_3\ (5-2x)SiO_2\ xLi_2O$ with x = .174 (about the limit of Li solubility) and Ge-doped: $2MgO\ 2Al_2O_3\ 4SiO_2\ GeO_2$ (nominal). The Li was added as $LiAlO_2$. The well mixed powders were melted in Pt crucibles, homogenized at 1650°C, quenched and devitrified, using procedures described elsewhere.[8] Devitrification temperatures were: 1000°C for 20 hrs for the Li and Ge doped samples and 1000°C for 24 hrs followed by 1100°C for 20 hrs for the pure sample. Samples were hand ground wet to ∿ -325 mesh. The Li-doped sample was ground in 1% HF solution for 15 mins to remove a small amount of $Li_2Al_2Si_3O_{10}$ (PDF #25-1183), then washed and filtered. Samples were checked for phase content, homogeneity and chemical composition by X-ray diffraction and SEM. All samples were homogeneous and essentially single phase hexagonal cordierite with no evidence of the orthorhombic form, i.e. no splitting or broadening of the (211) hexagonal peak at ∿ 29.5°2θ (CuKα).[6]

For the neutron work, approximately 12 gms of sample powder were packed into a thin walled vanadium can ∿ 5 cms long x 1.2 cms in diameter placed inside a Ta resistance furnace and mounted at the center of the general purpose powder diffractometer (GPPD) at the Intense Pulsed Neutron Source (IPNS) at Argonne National Lab. Details of this instrument and its operation are given elsewhere.[9,10,11] In brief, the source is a spallation type emitting pulses 30 times/sec. During each pulse, the neutrons arriving at the detectors of the GPPD have wavelengths, λ, which increase linearly with time, t. Equating the de Broglie relation to the Bragg law we obtain:

$$\lambda = \frac{ht}{mL} = 2d\ \mathrm{Sin}\theta \qquad (1)$$

Here h is Planck's constant, m the neutron rest mass, L the total neutron flight path from source to detector (21.46m) and d is a particular interplanar spacing. Fixed banks of detectors at 2θ near 90° and 159° are used and the neutron counts measured as a function of time from the start of each pulse (time-of-flight method), rather than as a function of angle. Thus from eq (1), d = C(θ)*t. Since the scattering angle is slightly different for each detector in a bank (the constant, C(θ) is slightly different), the counts for a particular d from all the detectors in a bank can be summed in real time and normalized to a particular scattering angle (90° or 159°), a technique known as time focussing. The range of d values covered in each pulse for the 159° bank was .38 to 2.86Å (4 to 30 msec). The resolution, Δd/d of the GPPD (measured as the FWHM of a peak in terms of d) is .25% independent of d, compared with ∿ 1% (at 2θ = 20°) and ∿ .2% (at 2θ = 80°) for conventional X-ray diffraction. An important advantage of the IPNS is that the incident beam intensity increases rapidly with decreasing time, i.e. with decreasing d, up to the top of the Maxwellian distribution of neutron energies in the incident beam. Furthermore, the neutron scattering lengths are constant and do not depend on sin θ/λ as scattering factors do for X-rays.

These features resulted in diffraction peaks being identifiable down to d ≈ .54Å, whereas the corresponding limit for cordierite with a conventional Guinier X-ray diffractometer and CuKα, radiation was d ≈ 1.27Å

($2\theta \simeq 75°$). Runs were made in vacuum ($< 10^{-5}$ torr) at temperatures from 21°C to 750°C. Each run was terminated when the number of counts at the top of the Maxwellian distribution for the time-focused 159° detectors reached 2000 (about 3 to 3.5 hrs with the accelerator beam current at $\sim$ 12 μA). The 159° diffraction spectra at each temperature were fitted to calculated patterns using the Rietveld method[12] modified for time-of-flight neutron data.[13,14]

The structural refinements were carried out in the P6/mcc space group, using the structural data of Meagher and Gibbs[2] as starting values. The final refinement at each temperature utilized 36 variables: lattice parameters (2), background (2), scale factor (1), profile halfwidth (2), coordinates not fixed by the space group of the 5 atoms in the asymmetric unit (7), extinction (1), occupancy of the T_1 and T_2 sites constrained by stoichiometry (1), and anisotropic temperature factors (20). The refinements done in several successive steps all converged to weighted profile discrepancy factors, R, of less than 5%. R is defined in eq (2):

$$R^2 = \sum_i w_i[Y_i(\text{obs}) - S*Y_i(\text{calc})]^2 / \sum_i w_i[Y_i(\text{obs})]^2 \qquad (2)$$

where Y_i(obs) and Y_i(calc) are the observed and calculated counts in the ith time channel, S is the overall scale factor for the calculated pattern and w_i a weighting factor for the ith channel.

The refined atom coordinates and lattice parameters were used to calculate all bond distances $\leq$ 4Å and all bond angles involving bond distances $\leq$ 3Å in the unit cell.

RESULTS AND DISCUSSION

A portion of the neutron diffraction pattern for the pure sample illustrating a typical fit obtained is shown in Fig. 1. Lattice thermal expansion data are shown in Fig. 2. The structure of hexagonal cordierite has been described elsewhere.[15,8] Briefly, the structure consits of 6-membered rings of T_2 (Si rich) tetrahedra stacked one above the other, forming c axis channels (Fig. 3). Adjacent rings are rotated $\sim$ 30° relative to each other about the c axis. Rings are linked to each other laterally and vertically by T_1 (Al rich) tetrahedra and M (Mg) octahedra. Viewed normal to the c axis, T_2 and M polyhedra alternate, as shown in Fig. 4.

Data from the refinements were examined to see which structural features were changing significantly with temperature. The complete data are listed elsewhere.[16] The M-O_1 bond lengths increased with a thermal expansion coefficient of $9.8 \pm 1 \times 10^{-6}$/°C for all 3 samples. The $O_1(1)$-T_2-$O_1(9)$ bond angle(defined in Fig. 4) decreased from room temperature to 750°C for all 3 samples (107.82° to 106.79° pure, 107.74° to 106.95° Ge doped, 108.22° to 107.5° Li doped). Similar changes were reported by Hochella et al.[17] in orthorhombic cordierite. The O_1-T_1-O_1 angles in tetrahedron T_1 changed as shown in Fig. 5. The T_1 and T_2 site occupancies did not change much for the Ge and Li doped samples (Table I) and became slightly more random with temperature for the pure sample. For the Ge doped sample, two models were tried: Ge associated with the Si (Si model) or with the Al (Al model). The Si model gave slightly better R values.

Fig. 1. A portion of the neutron powder diffraction pattern from d = .573 to 1.161Å for pure hexagonal cordierite at 22°C. (+) are the measured data, the solid line is the best fit profile and the vertical marks are the calculated positions of the reflections. A difference curve is shown at the bottom. Background was subtracted before plotting.

Fig. 2. Lattice thermal expansion of pure, Li-doped and Ge-doped hexagonal cordierites. Standard error bars on the individual points are 20 to 40 ppm.

Fig. 3. Projection along the c axis of the hexagonal cordierite (beryl) structure in space group P6/mcc. The five atoms in the asymmetric unit: T_1, T_2, M, O_1 and O_2 are shown together with the 3 basic polyhedra: T_2, T_1 and M from which the structure is built. Each tetrahedron T_1 shares 2 edges with adjacent M octahedra. Each M shares 3 edges with adjacent T_1's. Origin is at 0.

Fig. 4. Schematic representation of a portion of the hexagonal cordierite structure viewed normal to the c axis. Octahedra M and tetrahedra T_2 alternate along the c direction. Tetrahedra T_1 (which share edges with M) are not shown for clarity.

Table I: Fractional Al Occupancies in T_1 and T_2 (Si model). Standard deviations in the last digit are given in parentheses.

	Pure		Ge Doped		Li Doped	
Temp. °C	22	750	26	750	21	750
T_1	.70(7)	.52(10)	.53(3)	.55(5)	.85(8)	.85(10)
T_2	.32(3)	.41(5)	.40(2)	.39(5)	.24(4)	.25(5)

For the Li-doped sample, the Li content was too low to affect the refinement. A model with the Li in the c axis channels gave excessively large temperature factors for the Li; the Li was therefore omitted from the refinements other than to increase the Al/Si ratio.

Fig. 5. Changes in the O_1-T_1-O_1 bond angles in tetrahedron T_1 with temperature in pure and doped samples containing Ge and Li. (a) Angle subtended by the top or bottom edges of T_1 (the diagonal lines on T_1 in Fig. 3). (b) Angle subtended by the two free (unshared) edges of T_1. (c) Angle subtended by the two M-shared edges of T_1.

Fig. 6. Expansion components along c in pure and doped samples. (a) The height, H_M, of octahedron M along c. (b) The height, H_{T_2}, of the $O_1(1)$-$O_1(9)$ edge(parallel to c) in tetrahedron T_2. (c) $H_M + H_{T_2}$ compared with $c_o/2$ (dotted).

Expansion Behavior

The expansion of the structure was resolved into components parallel and normal to the c axis.[8] Expansion parallel to c consisted of expansion of heights H_M and H_{T_2} (defined in Fig. 4) as shown in Fig. 6. H_M decreased with temperature to a shallow minimum around 400°C for all 3 samples while H_{T_2} decreased with temperature above about 400°C. Thus both H_M and H_{T_2} are involved in the negative c axis expansion. The sum $H_M + H_{T_2}$ agrees well with half the c lattice parameter as shown in Fig. 6(c).

Expansion normal to c was conveniently expressed as the expansion of polygons in the basal plane of the unit cell, defined in Fig. 7. Changes in the areas of these polygons with temperature are shown in Fig. 8. It is evident that areas M and P expand with temperature for all 3 samples, while the area H of the six-membered rings stays constant or decreases slightly.

Fig. 7. Division of the basal plane area into hexagons, H, formed by the outermost (O_1) oxygens of a ring of T_2 tetrahedra, triangles M formed by the top or bottom surfaces of octahedra and parallelograms P bounded by H and M. The total area of one unit cell base = H + 2M + 3P.

Fig. 8. (a),(b),(c). Contributions of the polygons shown in Fig. 7 to the expansion of the unit cell base for the pure, Li-doped and Ge-doped samples. The sum: H + 2M + 3P of the contributions is compared with the cell base area calculated from the a_o lattice parameter in (d).

An alternate way of showing the expansion effects is shown in Fig. 9. Here displacements of the 750°C atom coordinates (in the basal plane) relative to coordinates at 22°C were magnified 20x to reveal the expansion effects. If expansion in the basal plane were isotropic, on the atomic scale, displacements of all atoms in Fig. 9 would be radial from the origin and would increase with increasing distance from the origin. This is clearly not the case.

Distortion of Polyhedra

From Fig. 9 it is evident that with increasing temperature the T_2 atom moves significantly inward towards the c axis channels for all 3 samples, rather than radially outward from the origin. The O_2 atoms also

Fig. 9. c Axis projection of the 3 basic polyhedra M, T_1 and T_2 at 22 and 750°C for (a) pure, (b) Li-doped, and (c) Ge-doped hexagonal cordierite. Displacements of the 750°C atom positions from the 22°C positions have been magnified 20X. Origin is at 0.

move inward towards the origin while the O_1 atoms in tetrahedron T_2 move small amounts approximately circumferentially about the origin. These movements produce changes in the bond angle distortion index, σ, for tetrahedron T_2, as shown in Fig. 10(b). σ is defined in eq. 3:[18]

$$\sigma^2 = \sum_{i=1}^{n} (\theta_i-\theta_o)^2/(n-1) \qquad (3)$$

where θ_i is the bond angle subtended by an edge of the distorted polyhedron at the interior atom, θ_o is the corresponding angle for the undistorted polyhedron (109.47° for a tetrahedron, 90° for an octahedron) and n is the total number of edges. σ passes through a shallow minimum around 400°C for the 3 samples. With increasing temperature above ∿ 500°C, the increasing σ correlates for all 3 samples with the decreasing H_{T_2} (Figs. 6(b) and 10(a)). One can envisage that the inward movement of T_2 lengthens the T_2-O_1 bonds causing the $O_1(1)$-T_2-$O_1(9)$ bond angle to decrease and

Fig. 10. Variation of the bond angle distortion index, σ, (degrees) with temperature for (a) tetrahedron T_2, (b) tetrahedron T_1 and (c) octahedron M.

H_{T_2} to decrease. The movement of T_2 with increasing temperature in Fig. 7 is approximately away from the Mg atom at M in all 3 cases. Possible reasons are discussed elsewhere.[8,16]

The distortion of the T_1 tetrahedron is much more severe than that of the T_2, and decreases with increasing temperature as shown in Fig. 10(a) and (b). The distortion is torsional about an axis parallel to c and passing through the T_1 atom such that one pair of O_1-T_1-O_1 bond angles (the pair subtended by the free edges of T_1) is much larger, at $\sim 124°$ than the second pair at $\sim 96°$, subtended by the M-shared edges (Fig. 5). The angles subtended by the top and bottom edges are relatively undistorted. The distortion of the M octahedra is also severe and increases with increasing temperature (Fig. 10(c)).

The cause of the M and T_1 distortions appears to be that the M and T_1 polyhedra form rings surrounding the rather rigid 6-membered rings of T_2 tetrahedra (Fig. 3). The circumference of the M-T_1 rings would be too small to fit around the 6-membered rings if the M and T_1 polyhedra were undistorted; to fit around the 6-membered ring the M and T_1 must be stretched circumferentially into their distorted shapes. Hence these polyhedra are extended in the circumferential direction and shortened in the c direction. M and T_1 are constrained to have the same heights in the c direction by the space group.

With increasing temperature, the M-O_1 bonds expand, relieving some of the torsional distortion in T, but increasing the distortion in M. Possible reasons for the negative expansion of H_M up to 400°C are discussed elsewhere.[8,16]

Effect of Dopant Cations

The Ge and Li doped samples had larger T_2 tetrahedra and larger H_{T_2} values (Fig. 6(b)) than the pure sample, due to the larger Ge^{+4} ion size and the increased Al/Si ratio in the Li doped sample. The average T_2-O bond lengths at room temperature were: 1.648Å pure, 1.655Å Li doped and 1.658Å Ge doped. The size of the 6-membered T_2 rings was also larger in the doped samples (Fig. 8(c)) for the same reason. As a result of the larger T_2 ring size, the distortion of the T_1 polyhedra was also larger in the doped samples (Fig. 10(b); however, the H_M values for all 3 samples were about the same (Fig. 6(a)). Evidently the expected decrease in H_M from the increased distortion has compensated for the expected increase in H_M from the larger T_1 cation size in the doped samples.

The changes in H_M and H_{T_2} with temperature are quite similar for the 3 samples. The Ge doped sample shows a slightly smaller negative contribution from H_M and a slightly larger one from H_{T_2} than the pure sample (Fig. 6). Experiments with dopants producing larger effects are in progress.

CONCLUSIONS

Lattice thermal expansion coefficients for the samples investigated are all very similar: pure; $\alpha_a = 2.781$, $\alpha_c = -1.351 \times 10^{-6}c^{-1}$, Li doped; $\alpha_a = 3.155$, $\alpha_c = -1.228 \times 10^{-6}c^{-1}$, Ge doped; $\alpha_a = 2.943$, $\alpha_c = -1.545 \times 10^{-6}c^{-1}$ from room temperature to 750°C.

The negative c axis expansion results from two contributing effects: (1) displacement of the T_2 cations generally inward towards the c axis channels and (2) changes in the distortion of the coupled T_1 and M polyhedra. Both contributions are present in all 3 samples with the first more dominant in the Ge doped sample.

The severe bond angle distortion of the T_1 and M polyhedra apparently results from the fact that these polyhedra form rings which are stretched around the circumference of the 6-membered rings of T_2 tetrahedra in the structure.

ACKNOWLEDGEMENTS

We are grateful to Deane Smith of The Pennsylvania State University, M. F. Hochella of Stanford and R. N. Kleiner of Coors Ceramics Co. for helpful discussions.

REFERENCES

1. W. Schreyer and J. F. Schairer, Compositions and Structural States of Anhydrous Mg-Cordierites: A Reinvestigation of the Central Part of the System $MgO-Al_2O_3-SiO_2$, J. of Petrology 2:324 (1961).
2. E. P. Meagher and G. V. Gibbs, The Polymorphism of Cordierite II: The Crystal Structure of Indialite, Can. Mineralogist 15:43 (1977).
3. G. V. Gibbs, The Polymorphism of Cordierite I: The Crystal Structure of Low Cordierite, Am. Mineralogist 51:1069 (1966).
4. J. B. Cohen, F. K. Koss, and G. V. Gibbs, An X-Ray and Neutron Diffraction Study of Hydrous Low Cordierite, Am. Mineralogist 62:67 (1977).
5. K. Langer and W. Schreyer, Infrared and Powder X-Ray Diffraction Studies on the Polymorphism of Cordierite, $Mg_2(Al_4Si_5O_{18})$, Am. Mineralogist 54:1442 (1969).

6. A. Putnis and D. L. Bish, The Mechanism and Kinetics of Al,Si Ordering in Mg-Cordierite, Am. Mineralogist 68:60 (1983).
7. A. Miyashiro, T. Iiyama, M. Yamasaki, and T. Miyashiro, Am. Jour. Sci. 253:185 (1955).
8. P. K. Predecki, J. Haas, J. Faber, Jr. and R. L. Hitterman, Structural Aspects of the Lattice Thermal Expansion of Hexagonal Cordierite, submitted to J. Am. Ceram. Soc.
9. J. Faber, Jr., Sample Environments at IPNS: Present and Future Capabilities, Revue Phys. Appl. 19:643 (1984).
10. S. R. MacEwen, J. Faber, Jr., and A. P. L. Turner, The Use of Time-of-Flight Neutron Diffraction to Study Grain Interaction Stresses, Acta Met. 31:657 (1983).
11. J. Faber, Jr. and R. L. Hitterman, High Resolution Powder Diffraction Studies at a Pulsed Neutron Source, to be published in Vol. 29, Advances in X-Ray Analysis.
12. H. M. Rietveld, J. Appl. Crystallogr. 2:65 (1969).
13. J. D. Jorgensen and F. J. Rotella, J. Appl. Crystallogr. 15:27 (1982).
14. R. B. Von Dreele, J. D. Jorgensen and C. G. Windosr, J. Appl. Crystallogr. 15:581 (1982).
15. E. P. Meagher and G. V. Gibbs, The Polymorphism of Cordierite II: The Crystal Structure of Indialite, Can. Mineralogist 15:43 (1977).
16. J. Haas, Mechanism of Lattice Thermal Expansion in Pure and Doped Cordierite, M.S. Thesis, Physics Dept., University of Denver, Denver, CO.
17. M. F. Hochella, Jr., G. E. Brown, Jr., F. K. Ross and G. V. Gibbs, High Temperature Crystal Chemistry of Hydrous Mg- and Fe-Cordierites, Am. Mineralogist 64:337 (1979).
18. K. Robinson, G. V. Gibbs, and P. H. Ribbe, Quadratic Elongation: A Quantitative Measure of Distortion in Coordination Polyhedra, Science 172:567 (1971).

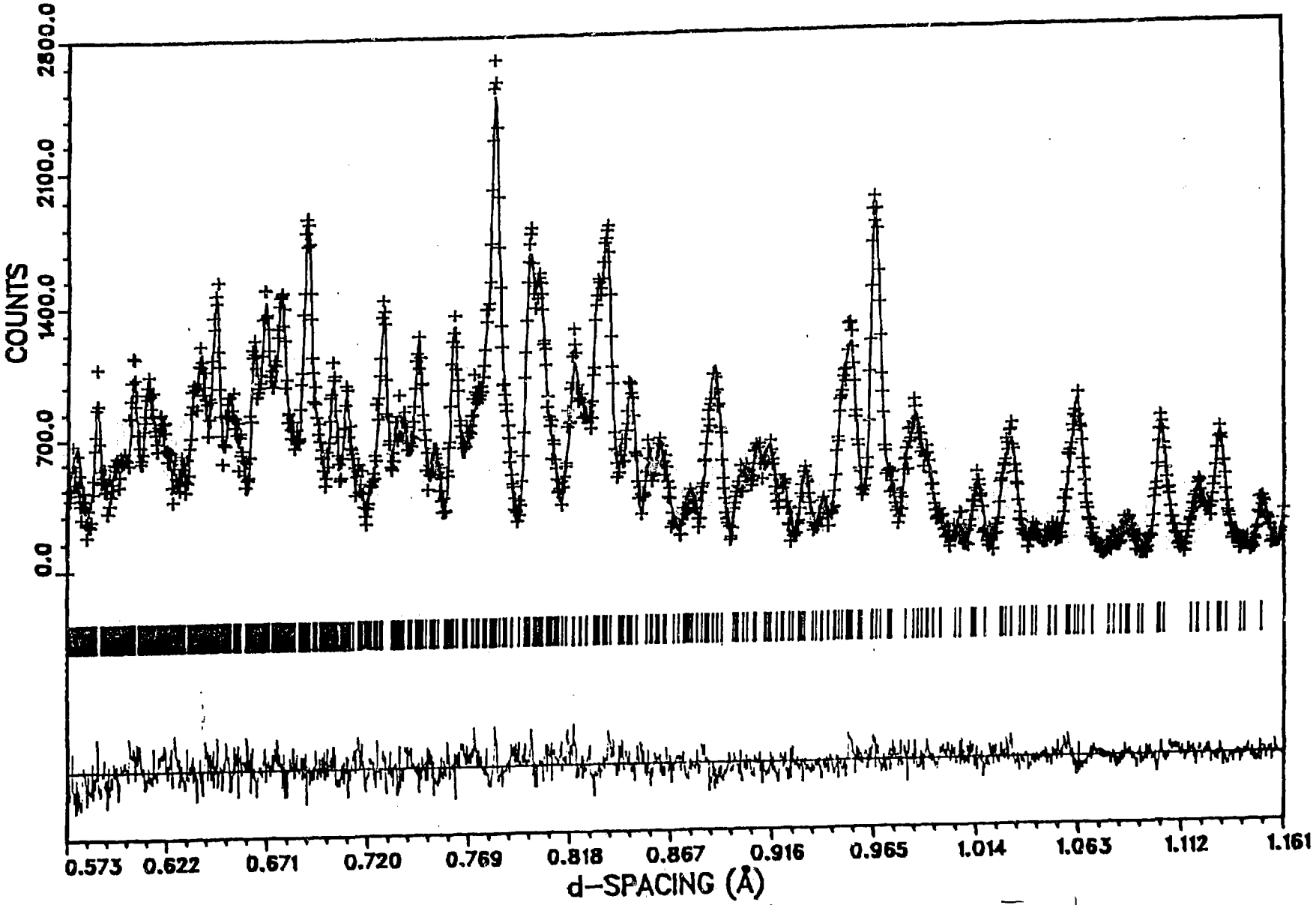
COUNTS
0.0
700.0
1400.0
2100.0
2800.0
0.573
0.622
0.671
0.720
0.769
0.818
0.867
0.916
0.965
1.014
1.063
1.112
1.161
d-SPACING (Å)

Fig. 1

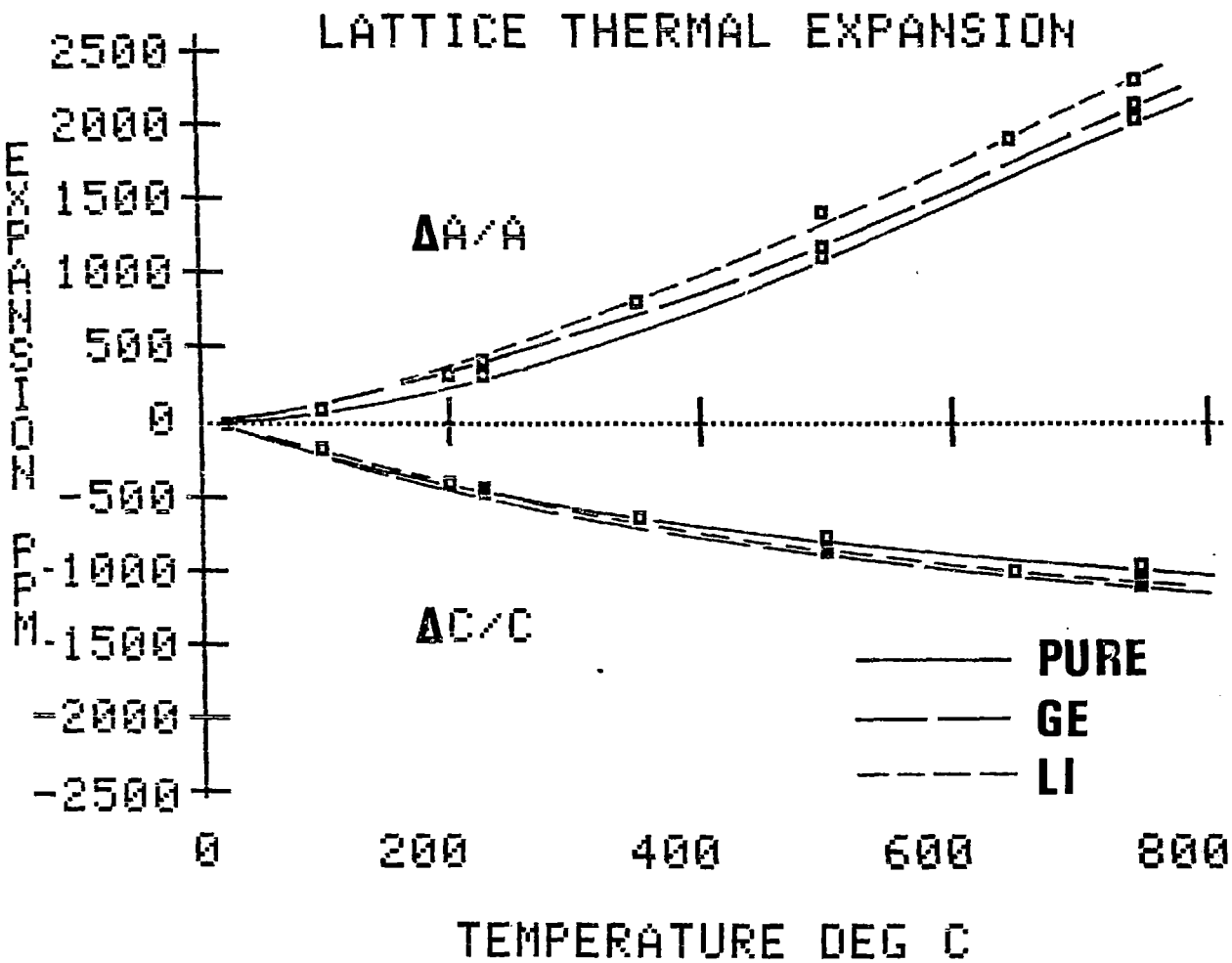
LATTICE THERMAL EXPANSION
2500
2000
1500
1000
500
0
-500
-1000
-1500
-2000
-2500
EXPANSION PPM
ΔA/A
ΔC/C
PURE
GE
LI
0
200
400
600
800
TEMPERATURE DEG C

Fig 2

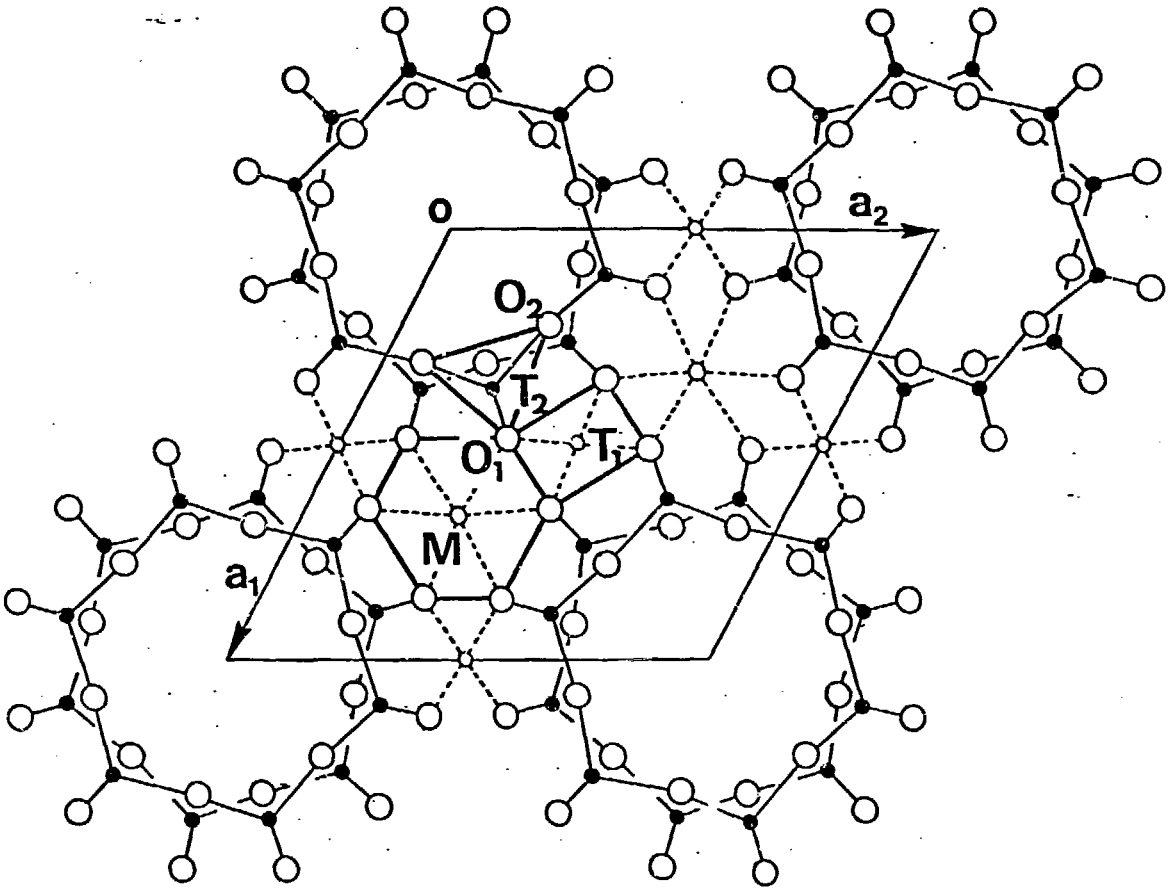

Fig 3

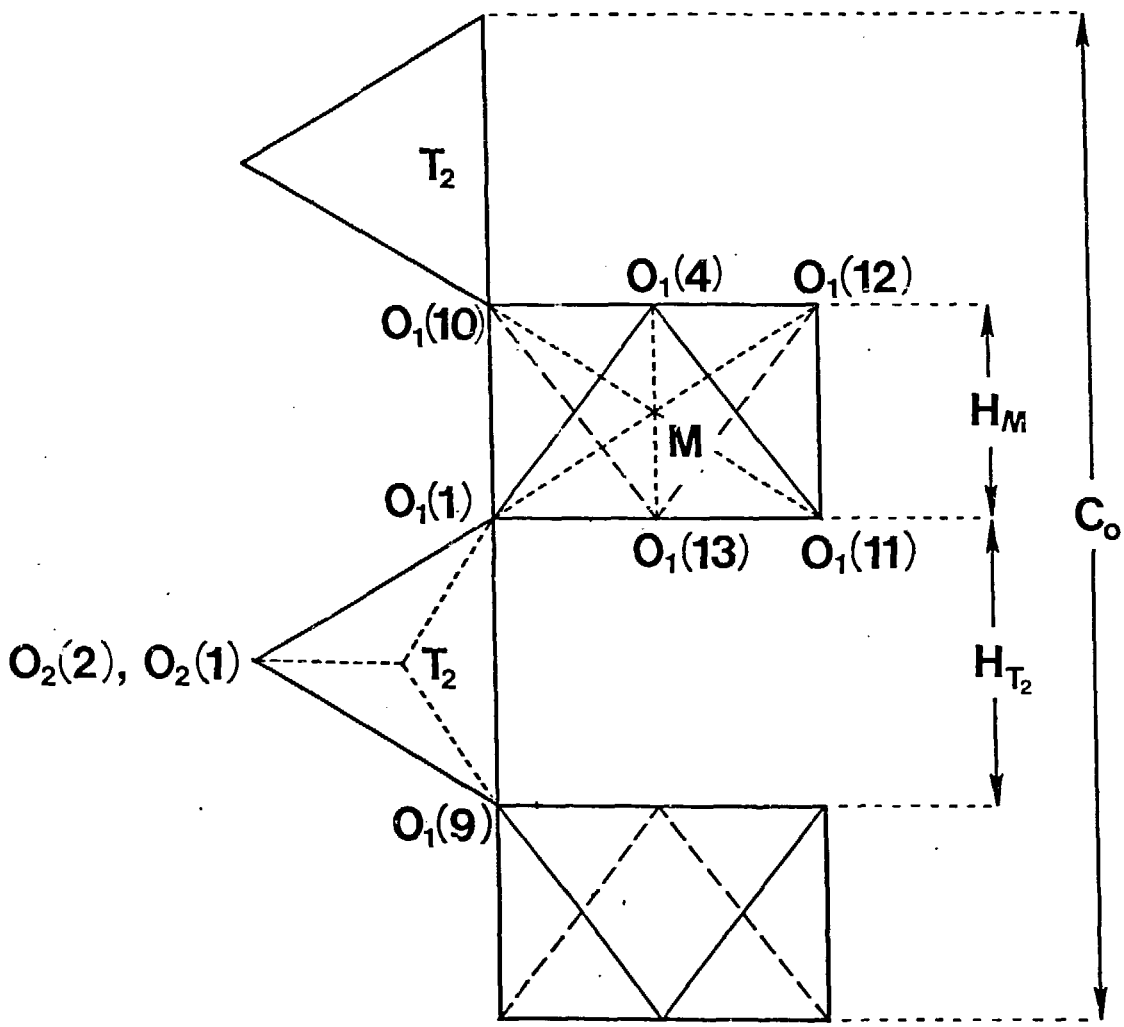

Fig. 4

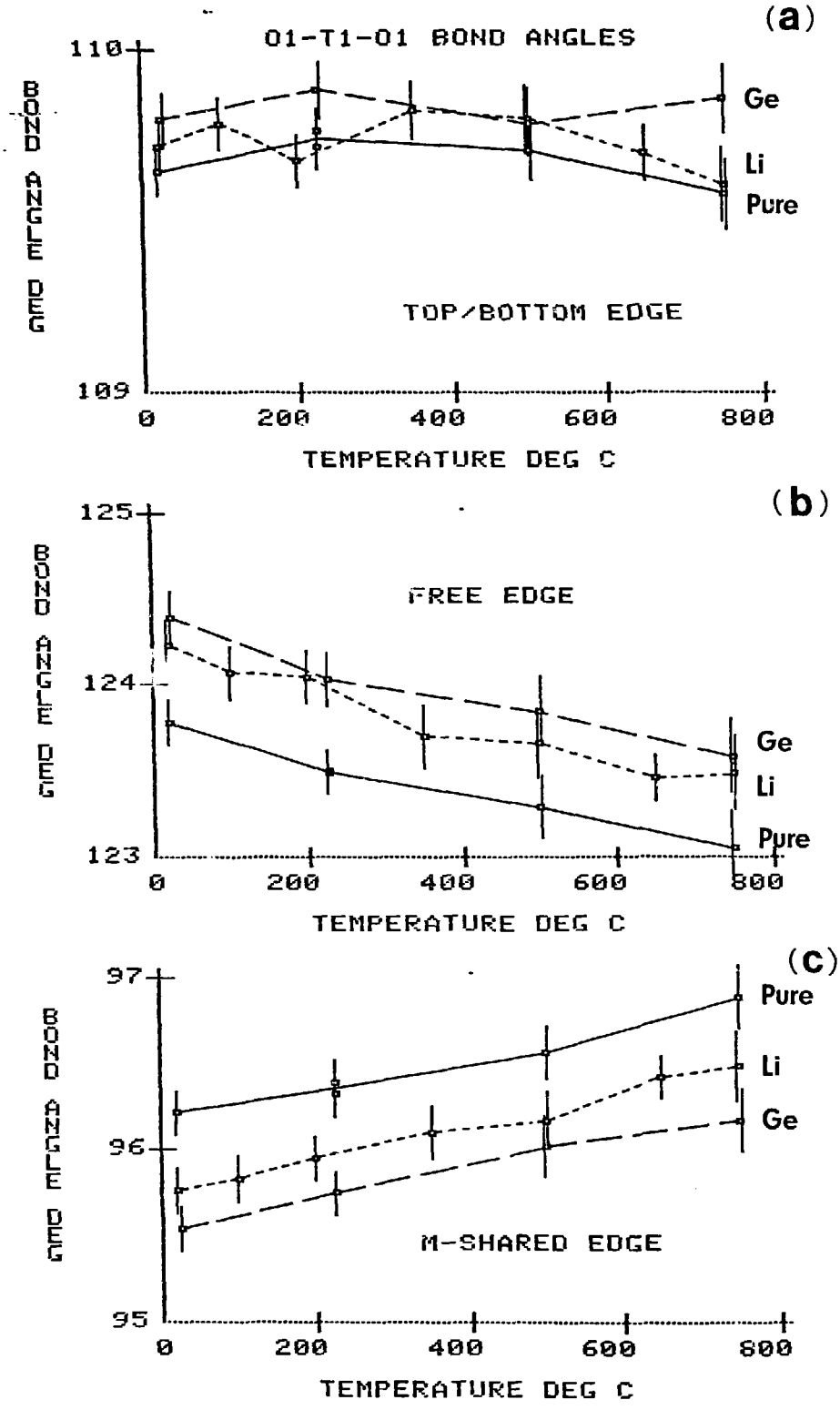
(a)
O1-T1-O1 BOND ANGLES
110
109
BOND ANGLE DEG
Ge
Li
Pure
TOP/BOTTOM EDGE
0
200
400
600
800
TEMPERATURE DEG C
(b)
125
124
123
BOND ANGLE DEG
FREE EDGE
Ge
Li
Pure
0
200
400
600
800
TEMPERATURE DEG C
(c)
97
96
95
BOND ANGLE DEG
Pure
Li
Ge
M-SHARED EDGE
0
200
400
600
800
TEMPERATURE DEG C

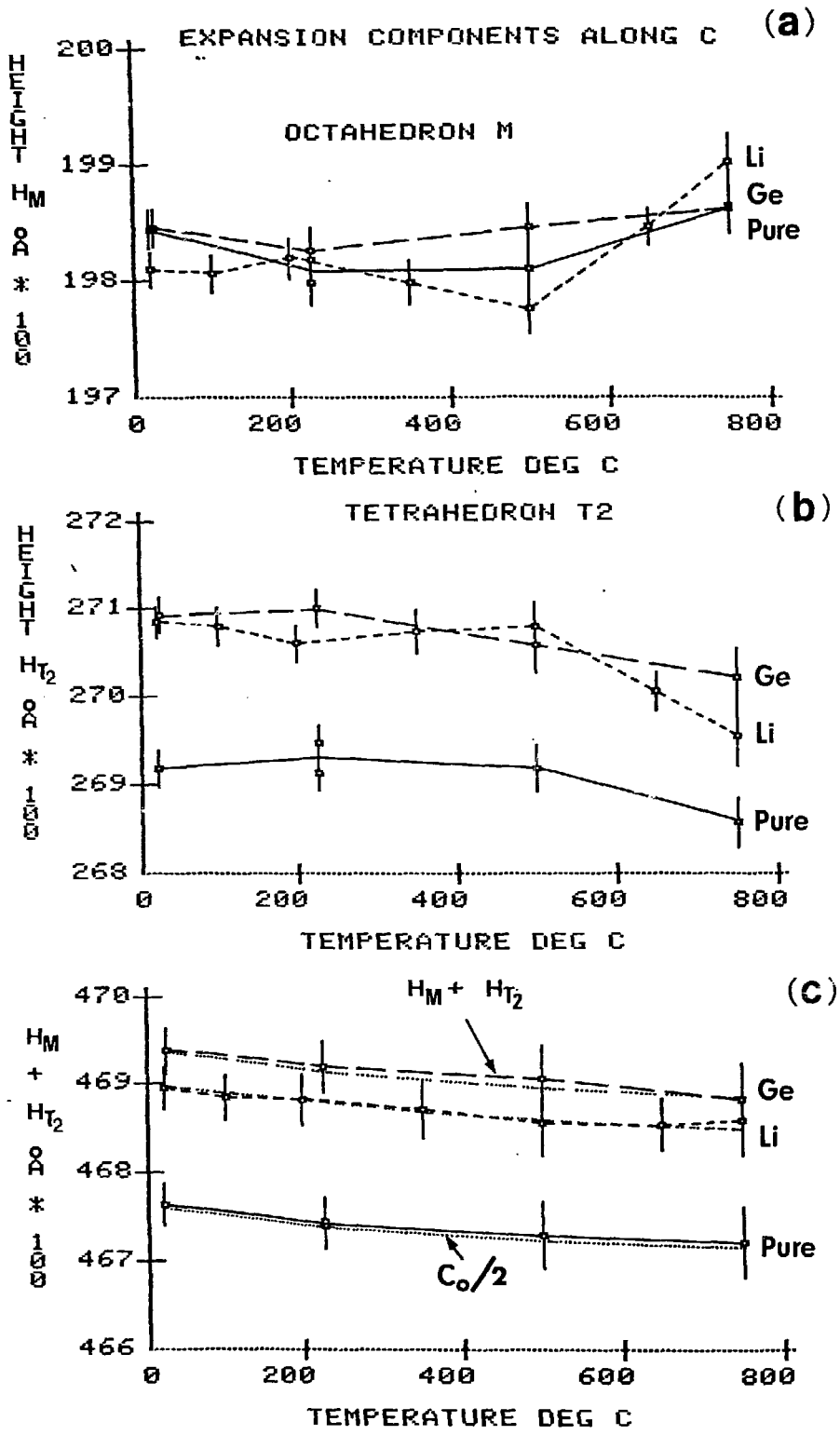
(a)
EXPANSION COMPONENTS ALONG C
OCTAHEDRON M
HEIGHT H_M Å * 100
200
199
198
197
Li
Ge
Pure
0
200
400
600
800
TEMPERATURE DEG C
(b)
TETRAHEDRON T2
HEIGHT H_{T_2} Å * 100
272
271
270
269
268
Ge
Li
Pure
0
200
400
600
800
TEMPERATURE DEG C
(c)
$H_M + H_{T_2}$
$H_M + H_{T_2}$ Å * 100
470
469
468
467
466
Ge
Li
Pure
$C_o/2$
0
200
400
600
800
TEMPERATURE DEG C

Fig. 6

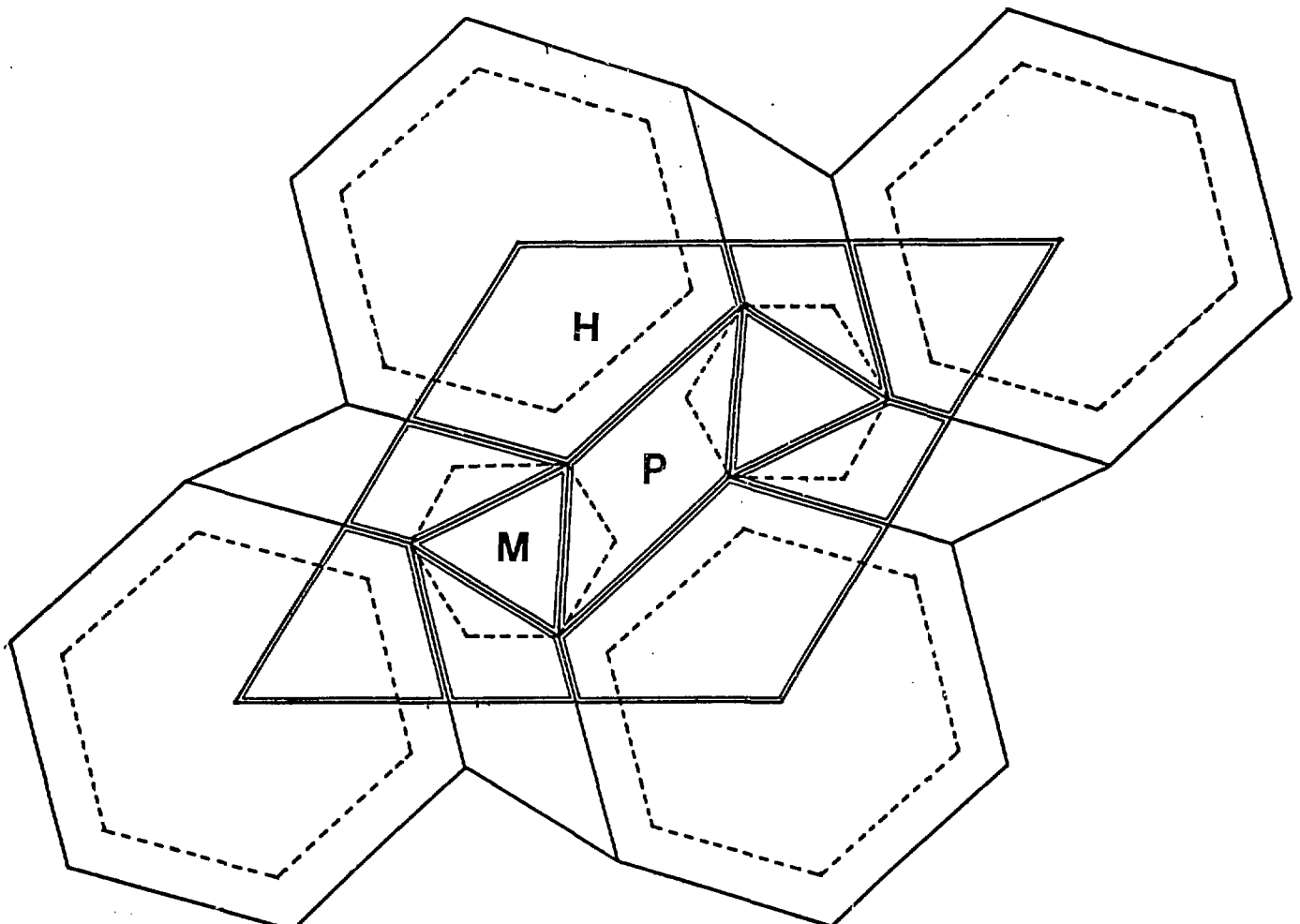
H
P
M

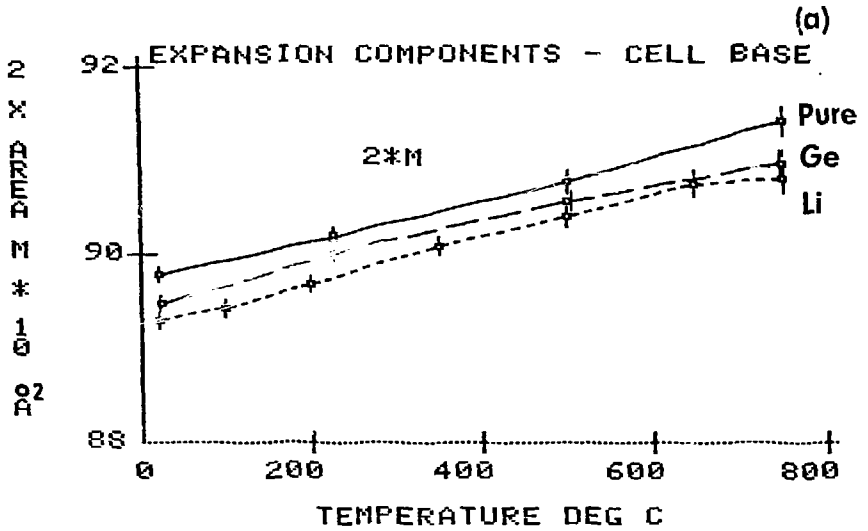
(a)
EXPANSION COMPONENTS - CELL BASE
2 X AREA M * 10 Å2
92
90
88
2*M
Pure
Ge
Li
0
200
400
600
800
TEMPERATURE DEG C

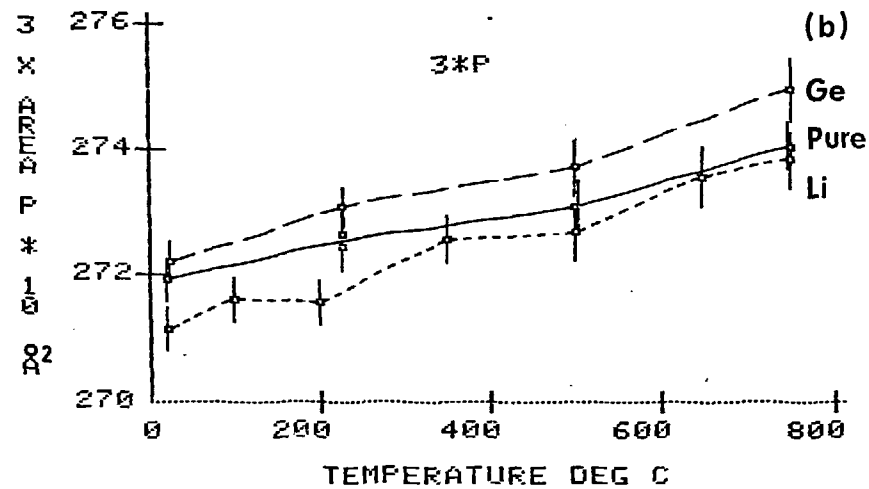
(b)
3 X AREA P * 10 Å2
276
274
272
270
3*P
Ge
Pure
Li
0
200
400
600
800
TEMPERATURE DEG C

Fig 2(a), (b)

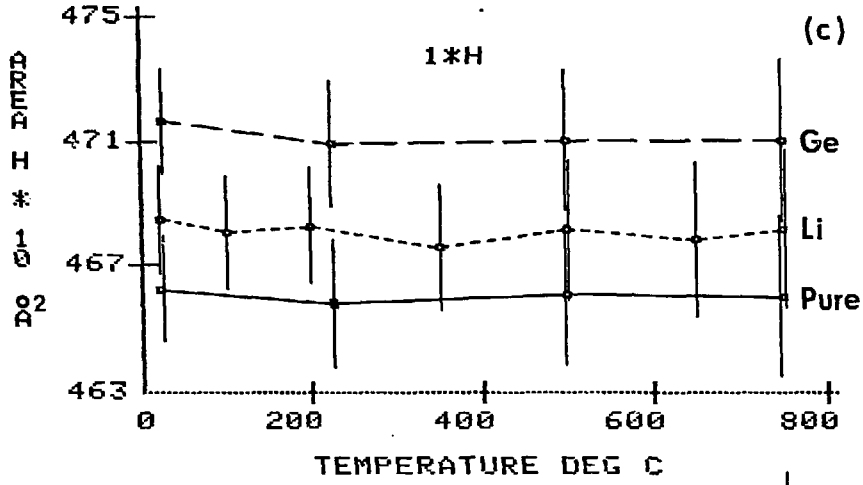
(c)
1*H
AREA H * 10 Å2
475
471
467
463
Ge
Li
Pure
0
200
400
600
800
TEMPERATURE DEG C

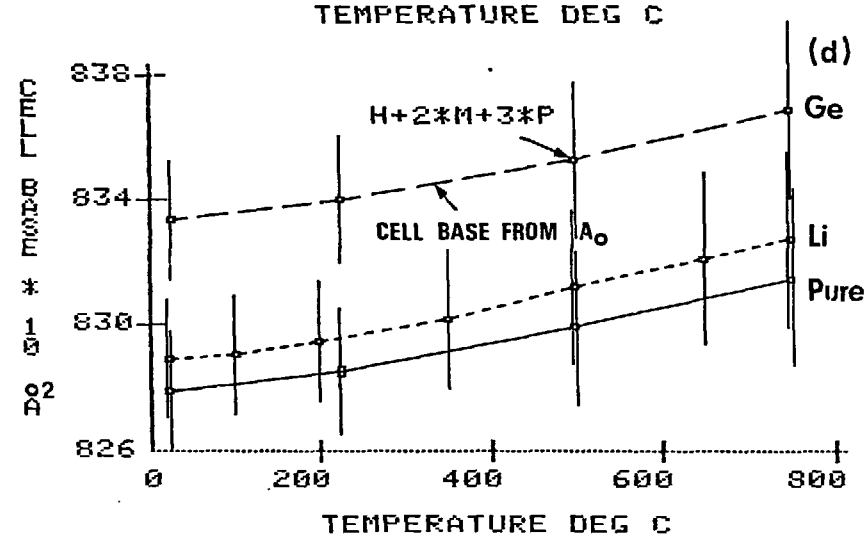
(d)
CELL BASE * 10 Å2
838
834
830
826
H+2*M+3*P
CELL BASE FROM Ao
Ge
Li
Pure
0
200
400
600
800
TEMPERATURE DEG C

Fig 8 (c), (d)

(a) Pure Cordierite

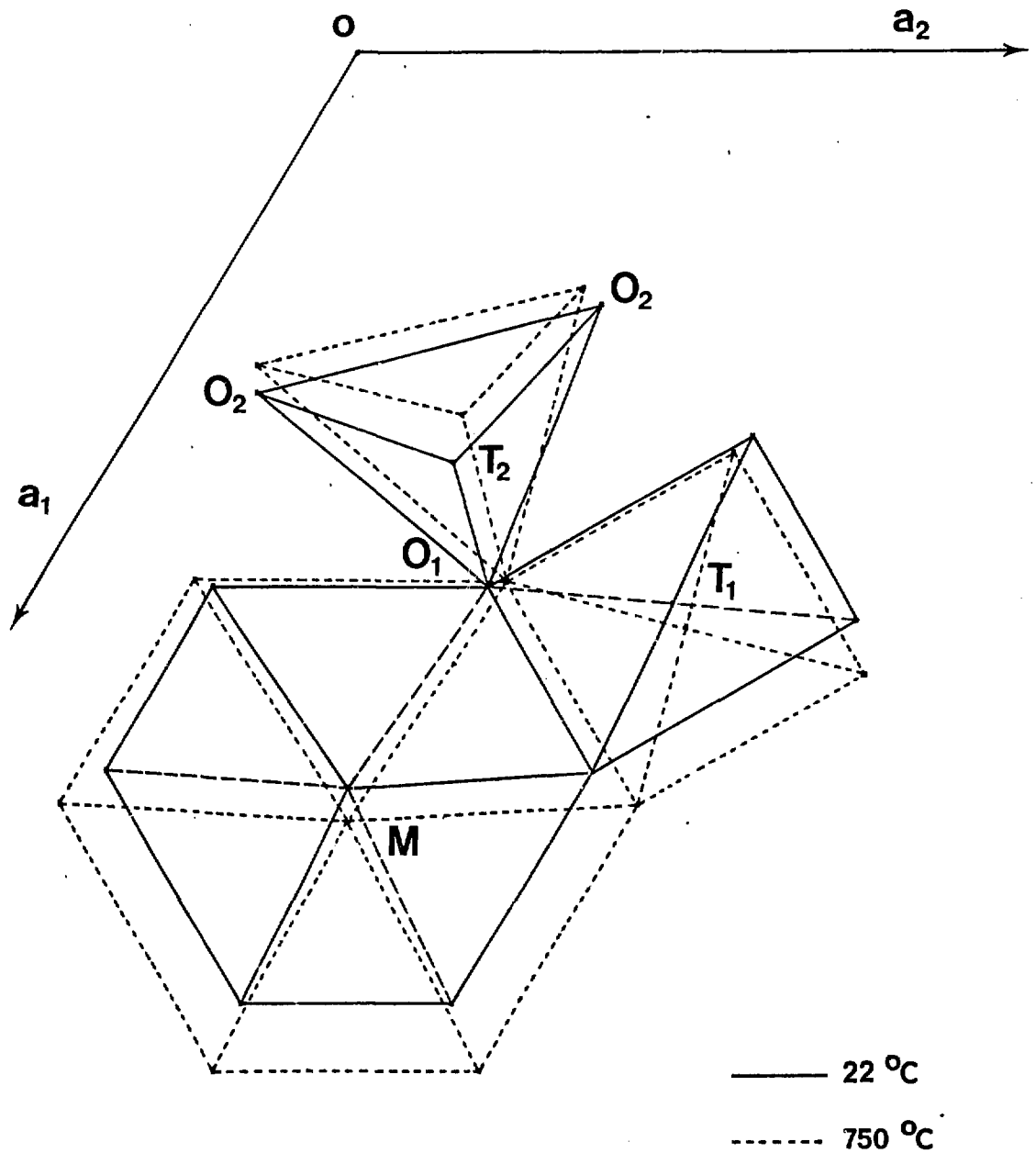

(b) Li doped Cordierite

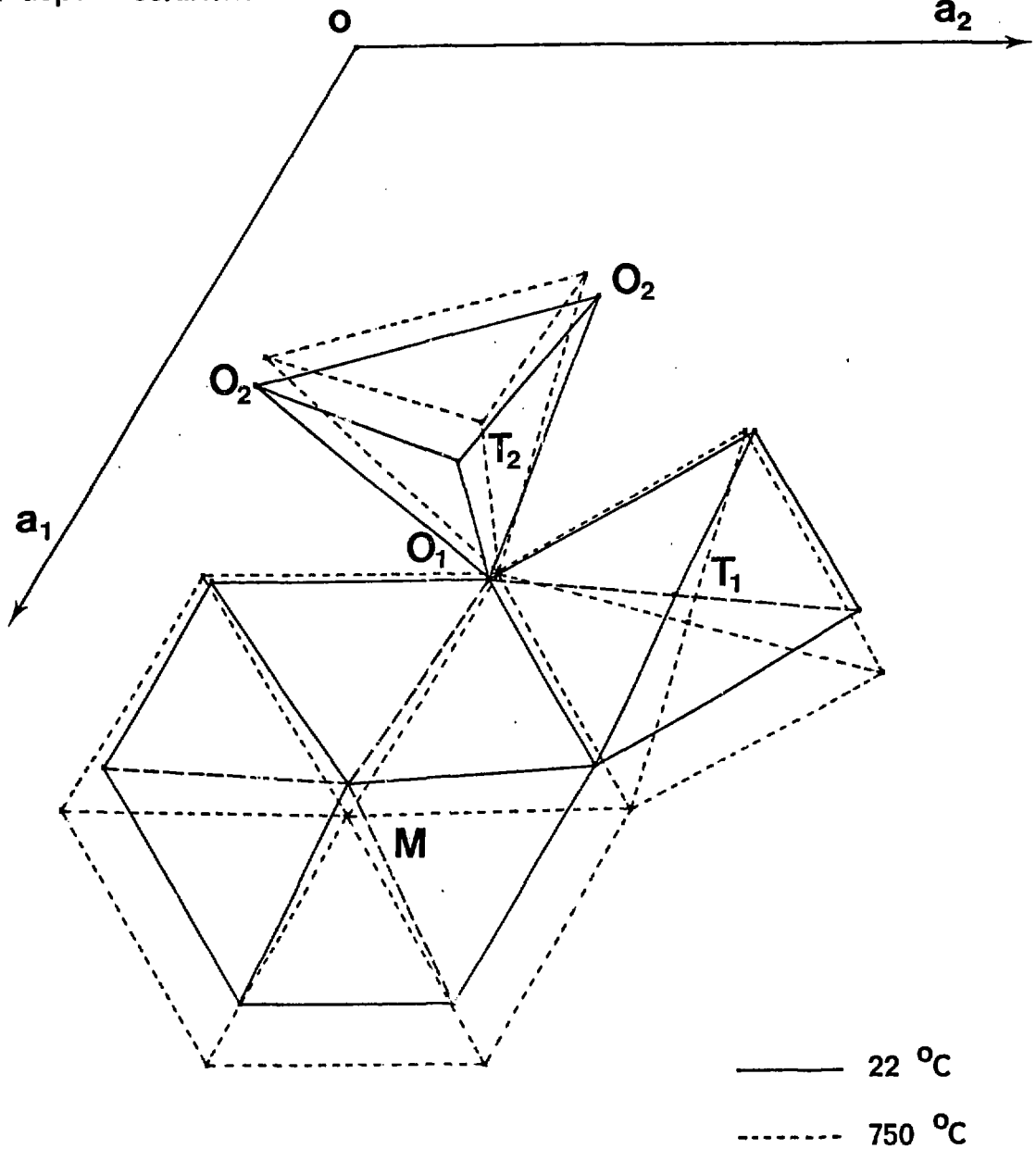

Fig. 9 (b)

(c) Ge doped Cordierite

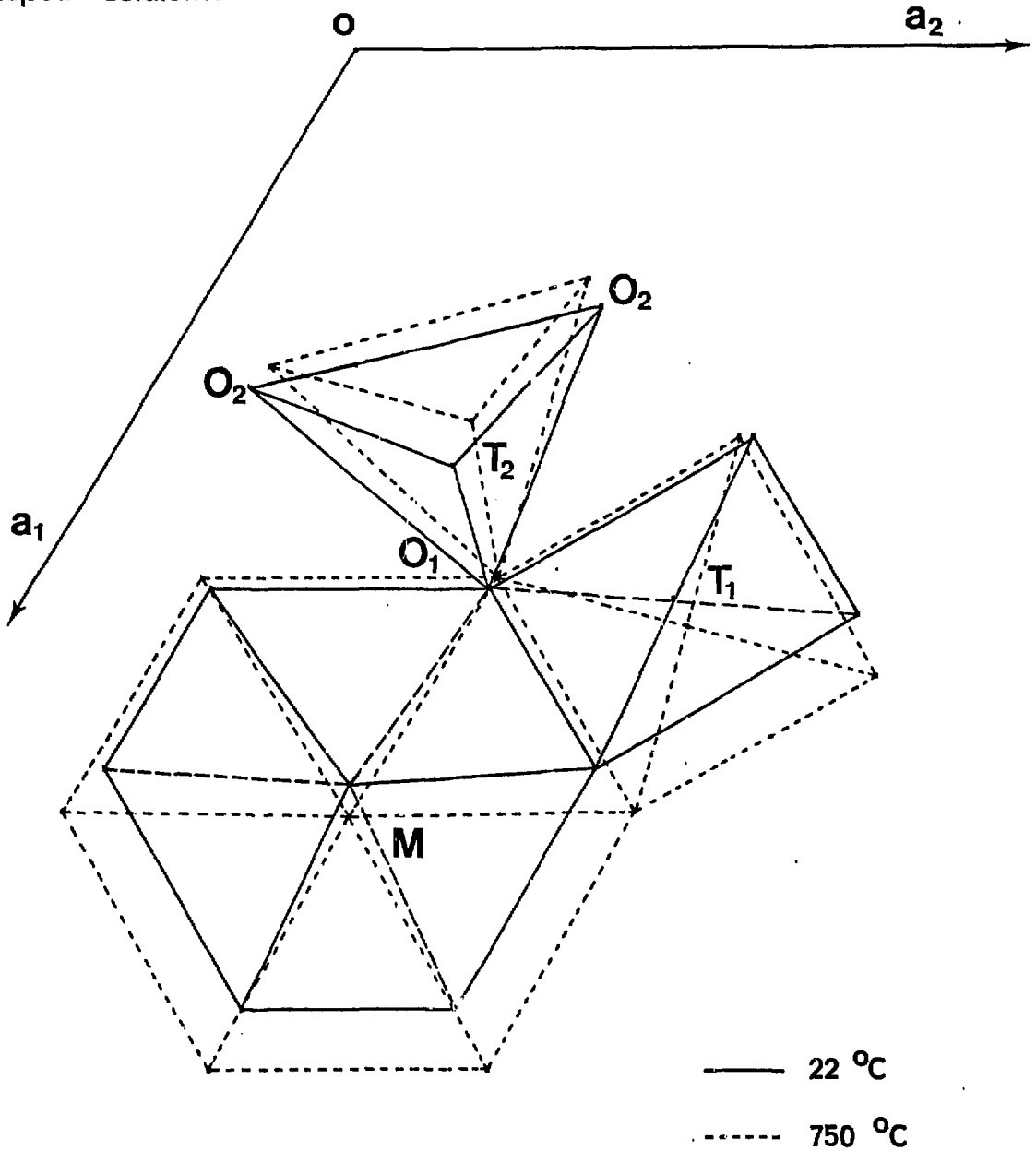

Fig. 9 (c)

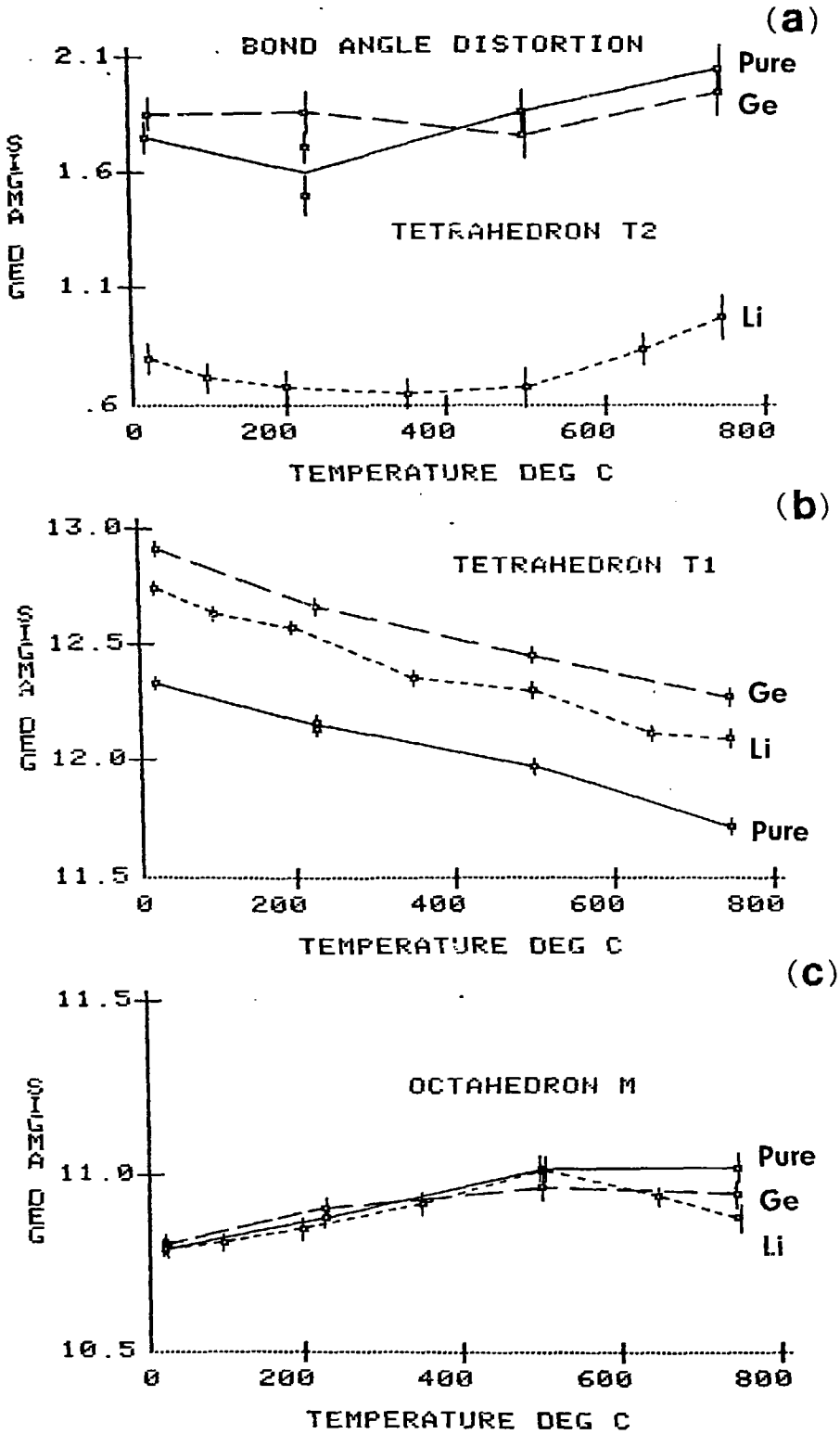
(a)
BOND ANGLE DISTORTION
2.1
1.6
1.1
.6
SIGMA DEG
Pure
Ge
TETRAHEDRON T2
Li
0
200
400
600
800
TEMPERATURE DEG C
(b)
13.0
12.5
12.0
11.5
SIGMA DEG
TETRAHEDRON T1
Ge
Li
Pure
0
200
400
600
800
TEMPERATURE DEG C
(c)
11.5
11.0
10.5
SIGMA DEG
OCTAHEDRON M
Pure
Ge
Li
0
200
400
600
800
TEMPERATURE DEG C